AD-A102 587 OKLAHOMA UNIV NORMAN SCHOOL OF AEROSPACE MECHANICAL --ETC F/G 11/10
EXPERIMENTAL INVESTIGATION OF THE MECHANICAL BEHAVIOR OF CORD-R--ETC(U)
JUL 81 N00014-78-C-0647
UNCLASSIFIED OU-AMNE-81-8 NL

1 OF 1
AD A
102587

END
DATE
FILMED
9-81
DTIC

LEVEL

12

ADA102587

Department of the Navy
OFFICE OF NAVAL RESEARCH
Structural Mechanics Program
Arlington, Virginia 22217

Contract N00014-78-C-0647
Project NR 064-609
Technical Report No. 23

Report OU-AMNE-81-8

EXPERIMENTAL INVESTIGATION OF THE MECHANICAL BEHAVIOR OF CORD-RUBBER MATERIALS

by

C.W. Bert and M. Kumar

July 1981

School of Aerospace, Mechanical and Nuclear Engineering
University of Oklahoma
Norman, Oklahoma 73019

Introduction

Experimental characterization means determination of the basic material properties by appropriate reduction of experimental data obtained from tests on suitable specimens [1]. In this investigation, only static mechanical properties [2] are considered. The main purposes for this information are:

(i) for research purposes (to check micromechanics analysis)

(ii) for design purposes (to generate data to be used in analysis and design of practical structural components)

Cords embedded in a rubber matrix comprise the class of composite materials of most commercial importance today in terms of total sales dollars. Their common uses are in products like pneumatic tires, power transmission belts, skirts for air cushion vehicles, and various kinds of hoses. The cord-rubber composites are also well known for having the special characteristics of significantly different stress-strain relations when loaded along the fiber direction in tension as opposed to compression [3]. Ambartsumyan [4] suggested that the stress-strain relations for such materials could be approximated to be bilinear, with one modulus when the fibers are stretched and another when they are compressed. Thus, these materials are sometimes called bimodular composite materials. Therefore, four elastic constants are required to completely describe the mechanical behavior of a single, thin, orthotropic layer when all the cords are loaded in tension; a different set of four apply to the same layer when it is loaded in such a way that all the cords are in compression. Previously, data obtained in [5] were reduced by the methods of Model 2 in [6] to obtain

complete in-plane bimodular elastic properties of aramid-rubber and polyester-rubber [7]. In actuality, however, the mechanical behavior of cord-rubber is more highly nonlinear than bimodular. Thus, complete stress-strain curves are desired. The purpose of this investigation is to experimentally determine the two sets of stress-strain behavior and elastic properties of a basic orthotropic layer of cord-rubber when the cords are in tension and compression. The properties determined are Young's moduli in cord and transverse directions, Poisson's ratios, shear moduli, and tensile strengths in the material-symmetry directions.

Conventional electric-resistance metallic strain gages (foil or wire types) cannot be used to measure the strains in cord-rubber composite since the strain magnitudes are, typically, 15 to 20 times greater than strain magnitudes encountered in the common engineering materials like metals, wood, or hard plastics. Also, the higher stiffness of strain gage material compared to the cord-rubber causes a localized stiffening effect in the specimen. Such stiffening reduces drastically the measured strain magnitudes [8]. In addition, the poor heat dissipation through the cord-rubber softens the area beneath the current-carrying resistance strain gages. This softening increases the measured strain magnitudes. Thus, a transducer to measure large rubber strains without the side effects mentioned above is needed. Clip gage, rubber-wire gage, and liquid-metal strain gage (mercury gage) are the three transducers which meet these requirements [9]. Also, the Moiré method with photographic deposition of grids has been successfully used [5]. In this program, the liquid-metal strain gage is chosen to measure the strains due to the fact that it is easier to fabricate, calibrate, and use than the other transducers.

The three unidirectional cord-rubber composites that are characterized in this investigation are aramid-rubber, steel-rubber, and polyester-rubber.

Fabrication of Liquid-Metal Strain Gages

The liquid-metal strain gage (mercury gage) operates on the same physical principle as the conventional electric resistance strain gage: resistance change with applied strain. This gage is made up of a silastic tube of small diameter containing liquid mercury, which is sealed inside. Any change in the length of the tube causes a change in resistance of the mercury which, in turn, can be related to the applied strain. The silastic tube used to make the gages is porous to air and was obtained from Parks Electronics Laboratory, Beaverton, Oregon. The porosity allows the air to occupy any possible vacuum space created as the tube is stretched.

The silastic tube was cut into lengths of about 30.0 mm. The tip of a syringe containing mercury was inserted into one end of the tube and the piston was slowly pushed such that the tube was filled completely by mercury without any air pockets. The tube could be checked for air pockets by visual inspection, since the tube was nearly transparent. Then the other end of the tube was sealed with a copper wire of slightly larger diameter than the inner diameter of the tube. By checking the electrical continuity between the copper wire and the tip of the syringe, one ensured that there were no air pockets in the tube. Then the syringe tip was removed and that end of the tube also was sealed with a copper wire. These copper wires were inserted so as to seal the mercury under little pressure and to make contact with it. A teflon heat-shrink tube was inserted at

each end of the tube and was shrunk by blowing hot air on it. This holds the tube tightly pressed against the contact wire and provides extra grip to the gage when it is stretched. Now the gage is ready and can be used after soldering the contact wires to the lead wires.

The final inspection was done by using an ohmmeter (Simpson, Model 312) on the R x 1 scale and stretching the gage up to approximately 15% of its relaxed length. Continuity should not be broken. Resistance varies from a fraction of an ohm to a few ohms.

Gages of two different lengths were made, the longer gage being about thrice the length of the shorter one. The longer gages were used to measure longitudinal strains and the shorter ones for transverse strains. The typical dimensions of a longer gage are shown in Fig. 1.

Strain-Gage Calibration and Verification

Calibration of the liquid-metal strain gages was carried out with a tensometer (Hounsfield, Serial No. W6771). Separate calibration curves were obtained for each gage. The gages were gripped over the teflon end tubes in wedge grips of the tensometer as shown in Fig. 2. The actual applied strain was calculated by knowing the gage length of the strain gage and the cross-head speed of the tensometer. The strain indicated by the gage was measured by a conventional strain indicator. The gage factor was set at an arbitrary value of 2.00 for all the gages. Since the resistance of a liquid-metal strain gage was less than an ohm, it was connected to the strain indicator (Vishay, Model P-250A) in series with a 120-ohm resistance. An electrical-resistance metallic-foil gage of 120 ohms (Kyowa, Type KFD-2-C1-11, gage length 2.0 mm) was used for this purpose.

No temperature compensation was used, since the tests in this study were run at room temperature and variation in the temperature was negligible.

Two calibration curves were obtained for each gage, one using the strain indicator and the other using a millivolt meter (Hewlett-Packard, Model 250B) to monitor the indicated output. Figure 3 shows a block diagram of the calibration set up with a millivolt meter. Since the linear range of the millivolt meter output was $\pm$ 250 mv, the calibration curve with millivolt meter could be obtained up to a maximum of only 25 mv. The sensitivity knob of the indicator was set at its maximum setting to get a sensitivity of approximately 0.2 μ strain/mv. Therefore, the calibration curve obtained with the millivolt meter was more precise and was used when the liquid-metal strain gages were required to measure small strain magnitudes, like transverse strains. Figure 4 depicts a typical calibration curve obtained with the strain indicator. This calibration curve can be represented quite accurately by the equation

$$\varepsilon_{ind} = 1.19(\varepsilon + 0.00165\ \varepsilon^2) \tag{1}$$

where ε is the actual strain in <u>milli</u>strain and ε_{ind} is the indicated strain in <u>micro</u>strain. Similarly a typical millivolt meter calibration can be represented as

$$v_{ind} = 8.00(\varepsilon + 0.0034\ \varepsilon^2) \tag{2}$$

where v_{ind} is the indicated voltage in millivolts and ε is as defined previously. Although the ε^2 effect is in agreement with Sikorra's prediction [10], its coefficients were considerably smaller (0.00165 and 0.0034) than his prediction (0.5).

The calibration curve while releasing the extension of the strain gage followed almost the same path as that obtained while going up, with very little hysteresis. That is to say, the indicated output for a given actual strain is the same whether the strain gage is being stretched or released. Thus, it was concluded that while stretching or releasing, the same calibration curve can be used, without significant error, to obtain the actual strain. For the gages fabricated by the method described, the calibration curves differed from one another by no more than 10%.

An additional test was conducted to verify the validity of strain measurements by liquid-metal strain gages. A gage was mounted on an aramid-rubber specimen with cords at 90° to the loading direction. The specimen was pulled in the tensometer. The strain was measured not only by the strain gage but also by noting the relative displacements between two particular points 30 mm apart along the specimen. A traveling microscope having a least count of 0.005 mm (Gaertner, Serial No. 2072P) was used to measure the relative displacements. The strains measured by these two methods are tabulated in Table 1. As can be seen, they agree quite well with one another.

Determination of Properties from Uniaxial Tensile Tests

The mechanical behavior in the material-symmetry directions was obtained by conducting quite basic experiments. These experiments generally revealed both the strength and stress-strain behavior of the material. The strength properties determined were:

F_L^t = longitudinal tensile strength in L direction (cords in tension)

F_T^c = transverse tensile strength in T direction (cords in compression)

From the stress-strain curves, the following properties (varying due to nonlinearity) can be obtained:

E_L^t = Young's m dulus in the cord direction

E_T^c = Young's modulus in the transverse direction (compressive cord strain)

$\nu_{LT}^t = -\varepsilon_T/\varepsilon_L$ for $\sigma_L = \sigma$ and all other stresses zero

$\nu_{TL}^c = -\varepsilon_L/\varepsilon_T$ for $\sigma_T = \sigma$ and all other stresses zero

To obtain the in-plane shear behavior and consequently the shear modulus G_{LT}^t with respect to the material-symmetry axes, an off-axis tension test at 45° was conducted.

In the experimental determination of the stiffness and strength properties of a layer, it is important to ensure the imposition of a uniform stress state in the specimen. Such loading is relatively easy for isotropic materials. However, for composite materials, the orthotropy often introduces coupling between normal stresses and shear strains when loaded in directions other than material-symmetry directions. Thus, to ensure obtaining the desired information, the following special precautions were taken:

- The specimens in the L and T directions were cut such that they were exactly parallel or perpendicular to the cords.
- The 45° specimens had a length-to-width ratio of 10 and the Pagano-Halpin correction for shear coupling [11] was applied (see Appendix A).

The latter requirement was needed to minimize the effect of coupling present between normal stress and shear strain so as to get a uniform state of

strain at the central portion of the specimen.

The quantities E_L^t, E_T^c, ν_{LT}^t, ν_{TL}^c, F_L^t, and F_T^c were all determined by carrying out uniaxial tensile tests on specimens cut at 0° and 90° to the 'L' direction. As is well known, the waisted (or dog-bone type) specimens for unidirectional composites give rise to premature failure at the ends by matrix shear due to cut fibers. Hence, straight specimens with end tabs were used. Figure 5 shows the specimen design used.

The liquid-metal strain gages were mounted such that only their teflon end tubes are bonded to the specimen as depicted in Fig. 6. This mounting procedure was used to simulate the conditions of gripping the gage during calibration. Silicone rubber glue manufactured by General Electric Company, Schenectady, New York, was used for bonding the gages. This rubber glue was selected to facilitate reusing the gages and also to avoid any possible reinforcing effects of the epoxy cements, which have higher moduli. The transverse strain, needed to compute the Poisson's ratio, was measured by using the smaller liquid-metal strain gage. This gage was mounted in the transverse direction after giving it a pre-extension of 20% of its relaxed length. Since the transverse strain due to axial tension is compressive, the pre-extension gets gradually released. To convert the indicated output to actual compressive strain, the same calibration curve obtained by stretching the gage was used.

The Young's modulus at 45°, E_1^t, was determined by performing a uniaxial tensile test on a specimen taken at 45° to the cord direction. In this experiment only longitudinal strain was measured by mounting the strain gage at the center of the specimen. Shear modulus G_{LT}^t was calculated by using the procedure described in Appendix A. This test method

is obviously not suitable for shear-strength determination.

All of the uniaxial tensile tests mentioned previously were conducted in the tensometer. The extension rate in all the tests was 0.5 mm/minute. The number of specimens tested for each property varied from two to three depending on the variation in the results.

Many of the liquid-metal strain gages were reused on different specimens. It was verified that the same calibration curve was valid for repeated uses of the gage. Also, it was observed that the longer gages were more durable and stable in electrical continuity than the shorter ones.

Determination of Properties from Sandwich-Beam Tests

Compression testing is one area of composite-material characterization for which many methods and specimen geometries have been proposed. For determining compressive properties of composite materials, the following specimen geometries have been successfully used [1]:

Flat coupon specimens with guided faces to prevent buckling

Short tube specimens (loaded either axially or by external pressure)

Short cylindrical and block specimens

Sandwich-beam specimens [12-14]

In this program, sandwich-beam specimens were chosen, since the cord-rubber composites used in this study were available only in the form of thin flat sheets. For each cord orientation (0°, 45°, and 90°), two specimens were tested.

Since cord-rubber material is known to be nonlinear, special equations for the data reduction were derived and are presented in Appendix B.

The cord-rubber composite facings were cut in a band saw and then their sides were ground to the desired width. The honeycomb core used was Hexcel 5052 aluminum, 4.76 mm (9.1875 in.) hexagonal cell size, 0.0508 mm (0.002 in.) wall thickness, 91.31 kg/m^3 (5.7 lb/ft^3) core density. The surfaces of the facings were roughened and cleaned with acetone. The facings and the honeycomb core were bonded together using liberal amounts of quick-setting epoxy resin. The sandwich beams in thc L and T directions were of 25.4 mm width and those at 45° direction were of 12.7 mm width, with the same thickness and length.

The quantities E_L^c, E_T^t, and ν_{LT}^c were determined from the data obtained from four-point bending tests on sandwich beams in the L and T directions. Figure 7 shows the dimensions of a sandwich beam under four-point bending test. The liquid-metal strain gages were mounted in the center portion of the beam. For measuring compressive strains, the strain gages were mounted with pre-extension. On the compressive side of the beam both longitudinal and transverse strains were measured. Figure 8 shows a sandwich beam ready for testing. The bending tests were conducted in an Instron universal testing machine (Model TTCMI-6).

Figure 9 depicts the four-point bending fixture used. During testing, the loads were applied on the beam through some metal pieces especially designed to prevent loading on lead wires of the strain gages and to distribute the load over a small area rather than over a line. The strain-gage readings were taken until the honeycomb core showed the signs of failure (either by local crushing or by shearing). It is to be noted that ν_{TL}^c was determined from the tensile results on 90° specimens.

The stress-strain curves were deduced from ε_{to} and ε_{co} versus M data by using eqs (13) and (16), Appendix B, to calculate σ_c and σ_t and eqs (19) and (20), Appendix B, to calculate ε_t and ε_c.

To obtain data for determining G^c_{LT}, a four-point bending test on a 45° sandwich-beam specimen was used to measure E^c_1. A sandwich-beam width of 12.5 mm was used in this test to obtain a higher aspect ratio. By putting the values of E^c_1, E^c_L, E^c_T, and ν^c_{LT} in the appropriate equations of Appendix A, one can calculate the value of G^c_{LT}.

Results and Discussion

Figures 10-12 show the typical stress-strain curves for aramid-rubber in the cord, transverse, and 45° directions, respectively. In these figures the stress-strain curves are classified as tensile or compressive according to the kind of strain in the cords and not according to the type of uniaxial load applied on the specimen. In Fig. 11, for example, the tensile stress-strain curve in the transverse direction is obtained by uniaxial compressive loading of a 90° specimen. This is because, as explained earlier, uniaxial compression loading of a 90° specimen causes the cords to be subjected to tensile strain. From similar reasoning, the compressive stress-strain curve in Fig. 11 is obtained from a tensile test on a 90° specimen.

As evidenced in Fig. 10, the tensile stress-strain curve in the cord direction is quite nonlinear in the region very close to the origin and increases in slope with increasing strain. If this portion near the origin is omitted, the stress-strain curve is basically a straight line over a wide strain range. This typical tensile behavior of cord-rubber composites is due to the fact that during the initial part of stretching, the cords

get straightened gradually and while straightening the stiffness increases and attains a steady value after some strain [15]. The cord-direction compressive stress-strain curve also exhibits this kind of nonlinearity near the origin. The nonlinearity in compression is of opposite sense to that in tension, i.e., the slope decreases with increasing strain until it reaches a constant value. This is also a typical characteristic of cord-rubber composites and is due to the tendency toward micro-buckling of the cords under compression, which reduces their stiffnesses [15].

The compressive portion of the stress-strain curve of Fig. 10 is limited by the failure initiation (a combined crushing and shear in vertical plane) in the honeycomb core of the sandwich beam, due to large deformations involved in the testing. The slopes of the stress-strain curves (Young's moduli) of Fig. 10 were measured in the linear portions.

As can be seen from Fig. 11, the initial parts of both the tensile and compressive stress-strain curves in the transverse direction are essentially straight lines. The slopes of these straight portions were measured to obtain the Young's moduli in the transverse direction. The Young's moduli at 45° direction were also determined by measuring the slopes in the initial portions of the stress-strain curves of Fig. 12.

Some of the strength properties and the two sets of elastic properties of aramid-rubber, when the cords are in tension and compression, are tabulated in Table 2. Here, the cord volume fraction was determined by measuring the cord diameter with the traveling microscope and using the formula

$$\text{cord volume fraction} = (\pi/4)(d^2n/t)$$

where d = cord diameter, t = ply thickness, and n = cord end count (ends

per unit length perpendicular to cords).

Also, Table 2 shows the comparison between the values of elastic properties determined experimentally in this program with those reported in [7] for a cord volume fraction of 0.14. The elastic properties reported in this reference were obtained from the experimental tensile-test results by Patel, et al. [5], using the approach developed for Model 2 in [6]. Keeping in mind the difference in the cord volume fractions, the comparison is quite good. This difference in cord volume fractions is the reason for the significant difference in values of the major Young's modulus in tension. Also, the values of G^t_{LT} and G^c_{LT} were obviously expected to be the same, but the differences between those values are aggravated by the shear-coupling correction (Appendix A), so the uncorrected values are also listed.

The percentage elongation at failure was determined by noting the initial and final distances between the wedge grips.

The stress-strain curves for polyester-rubber are shown in Figs. 13-15 and the properties are listed in Table 3, along with values from [7].

Figures 16-18 show the stress-strain curves for steel-rubber. Although the steel-rubber was expected to have the minimum of nonlinearity in the stress-strain curves near the origin, Fig. 16 shows it to be the maximum. It was observed that this was mainly due to a particularly large amount of waviness in the cords of the steel-rubber specimens. The mechanical properties of steel-rubber are listed in Table 4 and some of them are compared with those reported in [5]. The significant bimodular characteristics observed in the present investigation is also attributed to the waviness of the cords. The raw experimental data for all of the specimens tested

are given in Appendix D of [16].

The stress-strain curves in the material-symmetry directions of cord-rubber composites can be observed to be continuously increasing in slope. As indicated in [17], a relationship of the form $\sigma = K\varepsilon^n$ can be used as a nonlinear approximation; here K and n are real constants. Table 5 gives the values of the constants for all three of the materials considered in this study.

Concluding Remarks

The conclusions drawn from the liquid-metal strain-gage testing are:

1. The gage can be used for strain measurements up to at least 30% elongation on materials with low moduli.

2. Repeatability of the gage characteristics within about 10% can be obtained for a group of gages by the fabrication method described. This can be improved by employing more sophistication in the fabrication method.

In general, the liquid-metal strain gage appears to be a versatile strain-measuring device with many potential applications.

The stress-strain curves of cord-rubber composites in the cord direction indicate that the tensile and compressive portions, omitting a region very close to the origin, are basically straight lines of different slopes.

The close agreement between the stress-strain curves obtained by the sandwich-beam tests and those by the uniaxial tests proves the validity of the sandwich-beam test to determine the elastic properties. Using the equations presented in Appendix B, this test method is recommended for obtaining nonlinear tension and compression stress-strain curves simultaneously.

The good agreement of the values of elastic properties determined experimentally in this program with those in [7] shows that the approach developed for Model 2 in [6] is quite accurate.

Further work needs to be done to correlate the experimental results with nonlinear micromechanics theories, such as those of [15] and [18].

Acknowledgments

The authors acknowledge the financial support of the Perkinson fund of the College of Engineering, University of Oklahoma, and the Structural Mechanics Program, Office of Naval Research, Arlington, Virginia. The cord-rubber composite materials were generously provided by the Firestone Tire and Rubber Company, Central Research Laboratories. Cooperation and assistance in the experiments by Dr. R.J. Block and Mr. J. King, of the School of Chemical Engineering and Materials Science, are also acknowledged.

References

1. C.W. Bert, "Experimental Characterization of Composites," Chap. 9 (pp. 73-133) in Structural Design and Analysis, Part II, C.C. Chamis, ed., Vol. 8 of Composite Materials, L.J. Broutman and R.H. Krock, Academic Press, New York, 1975.

2. C.W. Bert, "Static Testing Techniques for Filament-Wound Composite Materials," Composites, Vol. 5, No. 1, Jan. 1974, pp. 20-26.

3. S.K. Clark, "The Plane Elastic Characteristics of Cord-Rubber Laminates," Textile Research Journal, Vol. 33, No. 4, Apr. 1963, pp. 295-313.

4. S.A. Ambartsumyan, "The Axisymmetric Problem of a Circular Cylindrical Shell Made of Material with Different Strength [Stiffnesses] in Tension and Compression," Izv. Akad. Nauk SSSR, Mekhanika, No. 4, 1965, pp. 77-85; Engl. transl., Nat. Tech. Info. Service Document AD-675312, Dec. 1967.

5. H.P. Patel, J.L. Turner, and J.D. Walter, "Radial Tire Cord-Rubber Composite," Rubber Chemistry and Technology, Vol. 49, 1976, pp. 1095-1110.

6. C.W. Bert, "Models for Fibrous Composites with Different Properties in Tension and Compression," ASME Journal of Engineering Materials and Technology, Vol. 99, No. 4, Oct. 1977, pp. 344-349.

7. S.K. Kincannon, C.W. Bert, and V.S. Reddy, "Cross-Ply Elliptic Plates of Bimodulus Material," Journal of the Structural Division, Proc. ASCE, Vol. 106, No. ST7, Proc. paper 15537, July 1980, pp. 1437-1449.

8. M.F. Beatty and S.W. Chewning, "Numerical Analysis of the Reinforcement Effect of a Strain Gage Applied to a Soft Material," International Journal of Engineering Science, Vol. 17, No. 7, 1979, pp. 907-915.

9. M.L. Janssen and J.D. Walter, "Rubber Strain Measurements in Bias, Belted Bias and Radial Ply Tires," Journal of Coated Fibrous Materials, Vol. 1, Oct. 197, pp. 102-117.

10. C.F. Sikorra, "High Elongation Measurements with Foil and Liquid Metal Strain Gages," Preprint No. 17.11-1-65, 20th Annual Conference and Exhibit, Instrument Society of America, Los Angeles, CA, Oct. 4-7, 1965.

11. N.J. Pagano and J.C. Halpin, "Influence of End Constraints in the Testing of Anisotropic Bodies," Journal of Composite Materials, Vol. 2, No. 1, Jan. 1968, pp. 18-31.

12. M.E. Waddoups, "Characterization and Design of Composite Materials," Composite Materials Workshop, S.W. Tsai, J.C. Halpin, and N.J. Pagano, eds., Technomic, Stamford, CT, 1968, pp. 254-308.

13. E.M. Lenoe, "Testing and Design of Advanced Composite Materials," Journal of the Engineering Mechanics Division, Proc. ASCE, Vol. 96, No. EM6, Dec. 1970, pp. 809-823.

14. M.J. Shuart and C.T. Herakovich, "An Evaluation of the Sandwich Beam in Four-Point Bending as a Compressive Test Method for Composites," NASA Technical Memorandum 78783, Sept. 1978.

15. C.W. Bert, "Micromechanics of the Different Elastic Behavior of Filamentary Composites in Tension and Compression," Mechanics of Bimodulus Materials, C.W. Bert, ed., ASME, New York, 1979, pp. 17-28.

16. M. Kumar, "Experimental Characterization of Mechanical Behavior of Cord-Rubber Composites," M.S. thesis, Mechanical Engineering, University of Oklahoma, Norman, OK, June 1981.

17. L.I. Zolotukhina and V.A. Kepetov, "The Elastic Moduli of Flat Rubber-Fabric Constructions in Elongation and Compression," Soviet Rubber Technology, Vol. 27, No. 1, Jan. 1968, pp. 42-44.

18. M. Cominou and I.V. Yannas, "Dependence of Stress-Strain Nonlinearity of Connective Tissues on the Geometry of Collagen Fibers," Journal of Biomechanics, Vol. 9, No. 7, 1976, pp. 427-433.

19. R.M. Jones, Mechanics of Composite Materials, McGraw-Hill, New York, 1975, pp. 52-53.

20. B.W. Rosen, "A Simple Procedure for Experimental Determination of the Longitudinal Shear Modulus of Unidirectional Composites," Journal of Composite Materials, Vol. 6, No. 4, Oct. 1972, pp. 552-554.

21. H.T. Hahn, "A Note on Determination of the Shear Stress-Strain Response of Unidirectional Composites," Journal of Composite Materials, Vol. 7, No. 3, July 1973, pp. 383-386.

22. A. Nadai, Theory of Flow and Fracture of Solids, Vol. 1, 2nd ed., McGraw-Hill, New York, 1950, pp. 357-358.

Appendix A. Determination of Shear Modulus with Respect to Material-Symmetry Axes by Use of Off-Axis and Material-Symmetry-Direction Uniaxial-Loading Data, Including the Pagano-Halpin Correction for Shear-Normal Coupling

The Young's modulus E_L^k in the cord direction, the Young's modulus E_T^k in in-plane direction transverse to the cords, and at least one of the Poisson's ratios should be known prior to use this method for determining G_{LT}^k. In the case of bimodulus composite materials, unlike in ordinary composite materials, it is very important to use either only tensile or only compressive properties. That is to say, for example, if the tensile properties are to be used, E_L^t, ν_{LT}^t obtained from a tensile test on a 0° specimen and E_T^t obtained from a compression test on a 90° specimen can be used to compute G_{LT}^t. If one wants to use ν_{TL}^t instead of ν_{LT}^t, the value of ν_{TL}^t obtained from the compression test on a 90° specimen should be used in association with the well-known reciprocal relation

$$\nu_{LT}^t/E_L^t = \nu_{TL}^t/E_T^t \qquad (3)$$

It is to be noted that in the compressive test on 90° specimen, the cords

are subjected to tensile strain.

Now, it is feasible to employ a uniaxial test on any angle coupon specimen for determing E_1^k, provided the following conditions are satisfied:

(i) In-plane shear deformations arising due to the normal stress-shear-strain coupling are permitted.

(ii) The strain in cords should be either tensile or compressive, depending upon whether tensile properties or compressive properties are going to be used in the eventual calculation of G_{LT}^k.

If the former condition is not satisfied, additional stress systems are induced at the ends which affect the uniform state of stress at the test section. This problem is obviated by using specimens of higher length-to-width ratio. The second requirement can be ensured by using an angle between the loading direction and the cord direction less than that derived in [6] which results in zero normal strains in the cords along their axes. In [6], it was shown that the angle θ_o, for which cord tension or compression vanishes even though the specimen is uniaxially loaded, is given by

$$\theta_o = \text{arc cot } [-S_{TL}^k/S_{LL}^k]^{\frac{1}{2}} = \text{arc cot } [\nu_{LT}^k]^{\frac{1}{2}} \tag{4}$$

For an orthotropic layer that is stressed in 1-2 coordinates oriented at an angle θ with respect to material-symmetry directions (L,T), the elastic compliances are given in terms of those in material-symmetry coordinates as (adapted from Jones [19]):

$$\bar{S}_{11}^k = S_{11}^k \cos^4\theta + (2S_{12}^k + S_{66}^k) \cos^2\theta \sin^2\theta + S_{22}^k \sin^4\theta \tag{5}$$

$$\bar{S}_{16}^k = (2S_{11}^k - 2S_{12}^k - S_{66}^k) \sin\theta \cos^3\theta - (2S_{22}^k - 2S_{12}^k - S_{66}^k) \sin^3\theta \cos\theta \tag{6}$$

$$\bar{S}_{66}^k = 2(2S_{11}^k + 2S_{22}^k - 4S_{12}^k - S_{66}^k) \sin^2\theta \cos^2\theta + S_{66}^k(\sin^4\theta + \cos^4\theta) \tag{7}$$

Here, the S^k_{ij} are the compliances with respect to the material-symmetry axes and can be expressed in terms of the engineering elastic coefficients as follows:

$$S^k_{11} = 1/E^k_L \quad , \quad S^k_{12} = -\nu^k_{LT}/E^k_L \quad , \quad S^k_{22} = 1/E^k_T$$
$$S^k_{66} = 1/G^k_{LT} \tag{8}$$

Here, E^k_L and E^k_T are the Young's moduli parallel and transverse to the cord direction, ν^k_{LT} is the Poisson's ratio which is the transverse strain per unit normal strain when loaded uniaxially in the cord direction, and G^k_{LT} is the shear modulus with respect to the L,T axes.

Setting $\theta = 45°$, the angle selected for the off-axis specimens used in this investigation, and using eqs (8) in eq (5), one obtains

$$1/G^k_{LT} = 4\bar{S}^k_{11} - (1/E^k_T) - (1 - 2\nu^k_{LT})/E^k_L \tag{9}$$

However, $\bar{S}^k_{11}$ is the true compliance value, not the apparent one, $(\bar{S}^k_{11})_{app}$, measured on a uniaxial coupon strip subject to uniform axial displacement. According to the approximate analysis of Pagano and Halpin [11], the two compliances are related by

$$\bar{S}^k_{11} = (\bar{S}^k_{11})_{app}/(1 - \eta) \tag{10}$$

where $C \equiv$ *specimen half-width*, $L \equiv$ specimen length between tabs, and

$$\eta \equiv \frac{6(\bar{S}^k_{16})^2}{\bar{S}^k_{11}[6\bar{S}^k_{66} + (\bar{S}^k_{11}L^2/C^2)]} \tag{11}$$

Eliminating the actual compliance $\bar{S}^k_{11}$ from eqs (10) and (11), one obtains the following quadratic equation in η:

$$\eta^2 - A\eta + B = 0 \tag{12}$$

where

$$A \equiv [2(\bar{S}^k_{16})^2 + \bar{S}^k_{66}(\bar{S}^k_{11})_{app} - (1/6)(\bar{S}^k_{11})^2_{app}(L/C)^2]/[(\bar{S}^k_{16})^2 + \bar{S}^k_{66}(\bar{S}^k_{11})_{app}]$$

$$B \equiv 1 + [\bar{S}^k_{66}(\bar{S}^k_{11})_{app}/(\bar{S}^k_{16})^2]$$

The data-reduction procedure is to use eqs (6) and (7) to calculate $\bar{S}^k_{16}$ and $\bar{S}^k_{66}$ from values of E^k_L, E^k_T, and ν^k_{LT} known from 0° and 90° specimens. Then, using these and $(\bar{S}^k_{11})_{app}$ measured directly from the 45° specimen, one can use eq (12) to obtain η. Thence, using eq (10) to determine $\bar{S}^k_{11}$ and finally using eq (9), one obtains G^k_{LT}.

In the most drastically shear-coupled case in this investigation, polyester-rubber in cord tension, the correction η was -0.162, which resulted in a 28.0% increase in G_{LT} over the uncorrected value (see Table 3).

After experimentally determining ν^k_{LT}, θ_o was computed using eq (4) for all the three materials considered in this study. It was found that an angle θ of 45° is safe for getting the same kind of cord strain as that of the uniaxial stress applied on the off-axis specimen. Also, this value for θ simplifies the calculations. Hence, θ was chosen as 45° in this study.

It should be mentioned that the procedure used here to obtain nonlinear shear response from an off-axis (45°) uniaxial test differs from that described in the literature for balanced, symmetric $\pm$ 45° laminates [20-21]. The disadvantage of the latter method is that it requires a laminate having a total number of plies which is a multiple of four, i.e., at least four plies. Its advantage is simplicity in the data reduction. The advantage of the present method is that it requires only a single-layer specimen.

One further remark concerns the difference between the nonlinearity typically exhibited by epoxy-matrix composites and the nonlinearity

exhibited by the cord-rubber composites investigated here. Epoxy-matrix composites are typically essentially linear to failure when loaded in uniaxial tension in the material-symmetry directions (0° and 90°), but highly nonlinear at 45° and in pure shear. Conversely, the present composites are nearly linear at 45° but nonlinear at 0° and 90°.

Appendix B. Determination of Stress-Strain Curves Using Data Obtained From a Bending Test on a Sandwich Beam

When a sandwich beam is subjected to four-point bending as shown in Fig. 7, the central portion of the beam is under pure bending moment, i.e., there is no shear force present. Figure 19 shows the geometry, strain kinematics, and stress distribution in the central portion of the beam.

The derivation presented here is analogous to that of Nadai's relations [22] for a homogeneous, rectangular-cross-section beam.

The following hypotheses are made:

(i) The beam is in pure bending, i.e., there is no shear force present.

(ii) Plane sections remain plan (in view of hypothesis (i), they also remain normal to the deflected middle surface).

(iii) The stiffness of the core material is negligible compared to that of the facings.

(iv) The facings are of the same material and thickness.

(v) The facings are relatively thin compared to the core depth, i.e., $t/h \ll 1$ (see Fig. 19).

(vi) The facing stress-strain curves in tension and compression may be different and nonlinear.

Equilibrium of horizontal forces requires that

$$\sigma_t t + \sigma_c t = 0$$

or

$$\sigma_c = -\sigma_t \tag{13}$$

Equating the externally applied bending moment M (per unit width) to the internal one gives

$$M = \sigma_t t[z_t - (t/2)] + \sigma_c t[z_c + (t/2)] \tag{14}$$

Substituting $\sigma_c = -\sigma_t$ from relation (13) into eq (14), one obtains

$$M = \sigma_t t[z_t - (t/2) - z_c - (t/2)] = \sigma_t t(z_t - z_c - t) \tag{15}$$

However, from Fig. 19, one finds that

$$z_t - z_c - t = h + t$$

Then eq (15) becomes

$$M = \sigma_t t(h + t)$$

or

$$\sigma_t = \frac{M}{(h + t)t} \tag{16}$$

To obtain the strain values corresponding to σ_t and σ_c, we need to convert the measured ones (ε_{to} and ε_{co}), which are measured at the outer fibers, to ε_t and ε_c. From Fig. 19, we have

$$\varepsilon_t = \varepsilon_{to}[1 - (t/2z_t)]$$

$$\varepsilon_c = \varepsilon_{co}[1 + (t/2z_c)]$$

Also, from the same figure,

$$z_t/\varepsilon_{to} = z_c/\varepsilon_{co} \tag{17}$$

$$z_t - z_c = h + 2t \tag{18}$$

Combining eqs (17) and (18), we obtain

$$z_t = \frac{h + 2t}{1 - (\varepsilon_{co}/\varepsilon_{to})} \quad , \quad z_c = (h + 2t)\left[\frac{\varepsilon_{co}/\varepsilon_{to}}{1 - (\varepsilon_{co}/\varepsilon_{to})}\right]$$

Thus,

$$1 - \frac{t}{2z_t} = \frac{h + 2t - (t/2) + (t/2)(\varepsilon_{co}/\varepsilon_{to})}{h + 2t}$$

$$= \frac{h + (t/2)[3 + (\varepsilon_{co}/\varepsilon_{to})]}{h + 2t}$$

$$1 + \frac{t}{2z_c} = \frac{h + 2t + (t/2)(\varepsilon_{to}/\varepsilon_{co}) - (t/2)}{h + 2t}$$

$$= \frac{h + (t/2)[3 + (\varepsilon_{to}/\varepsilon_{co})]}{h + 2t}$$

Finally, we obtain

$$\varepsilon_t = \varepsilon_{to} \left\{\frac{h + (t/2)[3 + (\varepsilon_{co}/\varepsilon_{to})]}{h + 2t}\right\} \tag{19}$$

$$\varepsilon_c = \varepsilon_{co} \left\{\frac{h + (t/2)[3 + (\varepsilon_{to}/\varepsilon_{co})]}{h + 2t}\right\} \tag{20}$$

It is important to note a significant difference between the data needed here for a sandwich-beam specimen and that needed for a solid rectangular specimen (or any other solid-section specimen)[22]. In the solid-specimen case, it is necessary to measure the beam deflection (or curvature) in addition to moment and the surface strains (ε_{co} and ε_{to}). Apparently, this advantage in simplicity in favor of sandwich-beam specimens to determining nonlinear stress-strain relations in tension and compression has escaped notice heretofore.

Table 1. Comparison of Strains Measured with Liquid-Metal Strain Gage and Traveling Microscope

Serial No.	Strain, mm/mm	
	Liquid-Metal Strain Gage	Traveling Microscope
1	0.024	0.0226
2	0.052	0.0542
3	0.075	0.0758
4	0.104	0.1001
5	0.123	0.119
6	0.153	0.1563
7	0.176	0.171
8	0.193	0.196

Table 2. Mechanical Properties of Aramid-Rubber

Cord Volume Fraction = 0.26

Property	Present	[7]
Properties for Cords in Tension		
Major Young's modulus (E_L^t), psi x 10^{-6}	0.41 I to 1.02 F[a]	0.519
(gigapascals)	(2.82 I to 7.03 F)	(3.58)
Minor Young's modulus (E_T^t), psi	1340	1320
(megapascals)	(9.24)	(9.09)
Major Poisson's ratio (ν_{LT}^t), dimensionless	0.40 I to 0.368 F	0.416
Shear modulus (G_{LT}^t), psi	832 I[b]	537
(megapascals) (corrected)	(5.74 I)	(3.70)
Cord-direction tensile strength, psi	25,860	-
(megapascals)	(178.0)	
Cord-direction elongation at failure, %	10.5	-
Properties for Cords in Compression		
Major Young's modulus (E_L^c), psi x 10^{-3}	32 I to 1.20 F	1.74
(megapascals)	(220 I to 8.26 F)	(12.0)
Minor Young's modulus (E_T^c), psi	1820 I	1740
(megapascals)	(12.5 I)	(12.0)
Major Poisson's ratio (ν_{LT}^c), dimensionless	0.19 I to 0.23 F	0.205
Minor Poisson's ratio (ν_{TL}^c), dimensionless	0.18 I to 0.197 F	-
Shear modulus (G_{LT}^c), psi	436 I[c]	537
(megapascals)	(3.00 I)	(3.70)
Transverse tensile strength, psi	1006	-
(megapascals)	(6.94)	
Transverse elongation at failure, %	228.0	-

[a] The symbol I denotes initial value and F denotes final value.
[b] Uncorrected value: 679 psi (4.68 MPa).
[c] Uncorrected value: 436 psi (3.00 MPa).

Table 3. Mechanical Properties of Polyester-Rubber

Cord Volume Fraction = 0.31

Property	Present	[7]
Properties for Cords in Tension		
Major Young's modulus (E_L^t), psi x 10^{-3} (gigapascals)	65 I to 110 F[a] (0.45 I to 0.76 F)	89.5 (0.617)
Minor Young's modulus (E_T^t), psi (megapascals)	1,050 (7.24)	1,160 (8.00)
Major Poisson's ratio (ν_{LT}^t), dimensionless	0.41 I to 0.37 F	0.475
Shear modulus (G_{LT}^t), psi (megapascals) (corrected)	759 I[b] (5.23 I)	380 (2.62)
Cord-direction tensile strength, psi (megapascals)	11,430 (78.8)	-
Cord-direction elongation at failure, %	21.1	-
Properties for Cords in Compression		
Major Young's modulus (E_L^c), psi x 10^{-3} (megapascals)	8.3 I to 5.3 F (57.3 I to 36.6 F)	5.35 (36.9)
Minor Young's modulus (E_T^c), psi (megapascals)	1,620 I (11.2 I)	1,540 (10.6)
Major Poisson's ratio (ν_{LT}^c), dimensionless	0.194	0.185
Minor Poisson's ratio (ν_{TL}^c), dimensionless	0.060	-
Shear modulus (G_{LT}^c), psi (megapascals)	380 I[c] (2.62 I)	387 (2.67)
Transverse tensile strength, psi (megapascals)	1,173 (8.1)	-
Transverse elongation at failure, %	295.0	-

[a] The symbol I denotes initial value and F denotes final value.
[b] Uncorrected value: 593 psi (4.09 MPa).
[c] Uncorrected value: 364 psi (2.51 MPa).

Table 4. Mechanical Properties of Steel-Rubber

Cord Volume Fraction = 0.157

Property	Present	[5]
Properties for Cords in Tension		
Major Young's modulus (E_L^t), psi x 10^{-6} (gigapascals)	0.30 I to 1.75 F[a] (2.1 I to 12.1 F)	2.04 (14.1)
Minor Young's modulus (E_T^t), psi x 10^{-3} (megapascals)	1.65 I to 0.89 F (11.4 I to 6.1 F)	-
Major Poisson's ratio (ν_{LT}^t), dimensionless	0.40 I to 0.39 F	-
Shear modulus (G_{LT}^t), psi (megapascals) (corrected)	425 I[b] (2.93 I)	453 (3.12)
Cord-direction tensile strength, psi (megapascals)	22,690 (156)	-
Cord-direction elongation at failure, %	6.24	-
Properties for Cords in Compression		
Major Young's modulus (E_L^c), psi x 10^{-3} (megapascals)	300 I to 154 F (2,100 I to 12,100 F)	-
Minor Young's modulus (E_T^c), psi (megapascals)	1,400 I to 100 F (9.06 I to 0.69 F)	1,451 (10.0)
Major Poisson's ratio (ν_{LT}^c), dimensionless	0.21	-
Minor Poisson's ratio (ν_{TL}^c), dimensionless	-	-
Shear modulus (G_{LT}^c), psi (megapascals)	478 I[c] (3.30 I)	-
Transverse tensile strength, psi (megapascals)	1,310 (9.04)	-
Transverse elongation at failure, %	122	-

[a] The symbol I denotes initial value and F denotes final value.
[b] Uncorrected value: 405 psi (2.79 MPa).
[c] Uncorrected value: 424 psi (2.92 MPa).

Table 5. Constants K and n in the Power-Law Expression $\sigma = K\varepsilon^n$, where ε is in in./in.

Material	Loading Direction	K, psi (MPa)		n	
		C.T.*	C.C.	C.T.	C.C.
Aramid-rubber	Cord	1.10×10^6 (7,580)	3,980 (27.4)	1.22	0.56
Aramid-rubber	Transverse	1,280 (8.82)	1,720 (11.9)	1.00	0.99
Polyester-rubber	Cord	5.52×10^5 (3,800)	5,600 (38.6)	1.12	0.90
Polyester-rubber	Transverse	1,000 (6.89)	567 (3.91)	1.00	0.71
Steel-rubber	Cord	22.0×10^6 (1.52×10^5)	33,000 (227)	1.74	0.63
Steel-rubber	Transverse	867 (5.97)	801 (5.52)	0.80	0.83

*C.T. denotes cords in tension, C.C. denotes cords in compression.

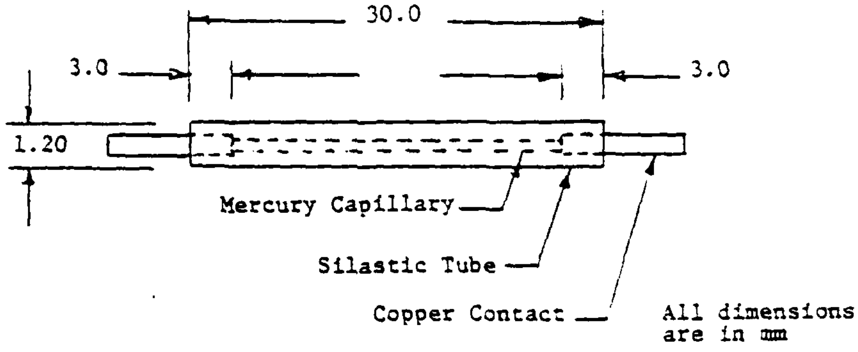

Fig. 1. Typical dimensions of a liquid-metal strain gage used to measure longitudinal strains (internal diameter of the tube = 0.40 mm).

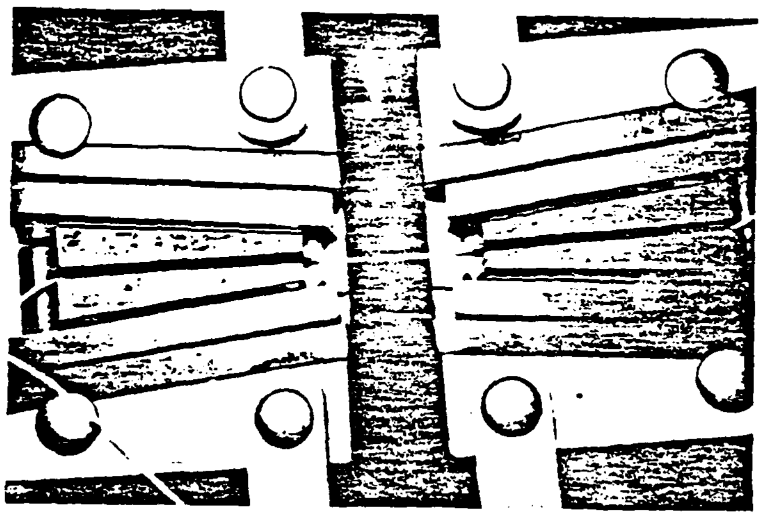

Fig. 2. Gripping of liquid-metal strain gage for calibration.

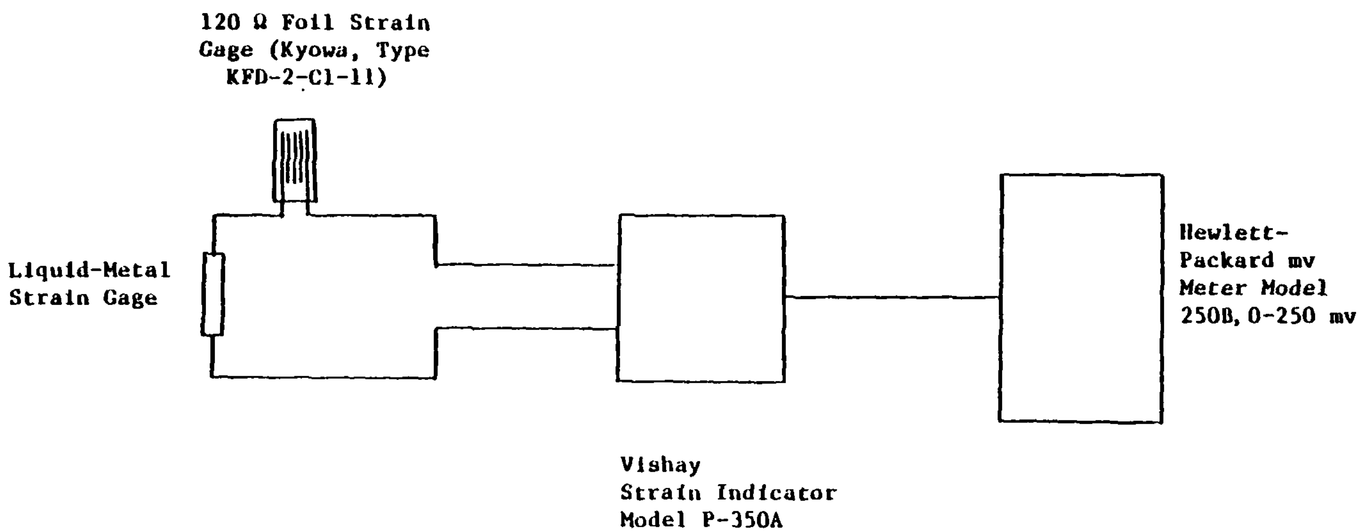

Fig. 3. Block diagram of the calibration setup.

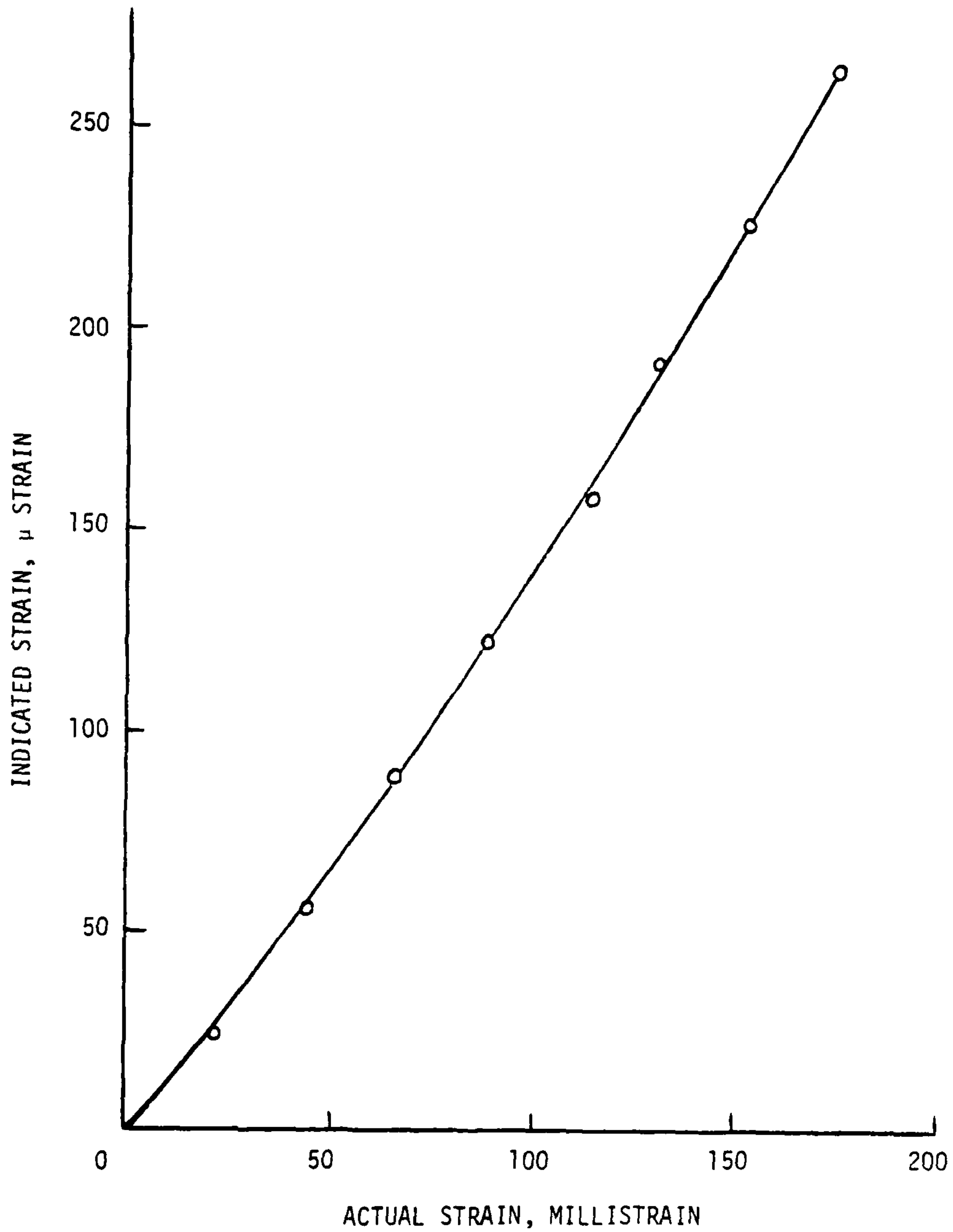

Fig. 4. Calibration curve for liquid-metal strain gage with strain indicator.

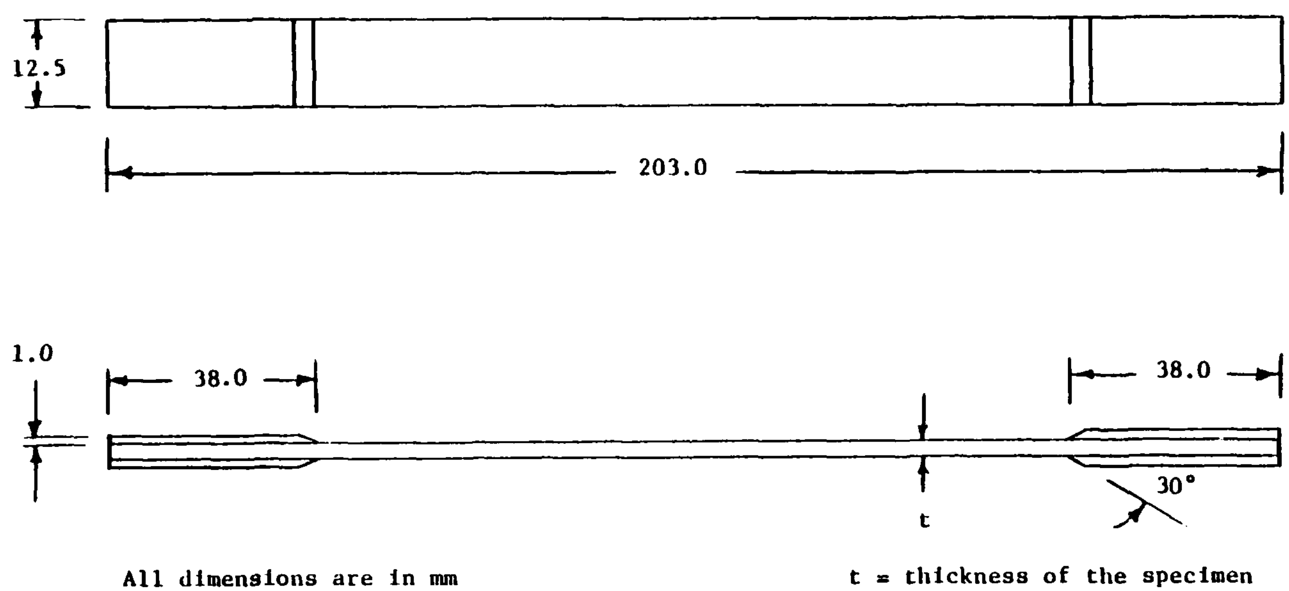

Fig. 5. Tensile test specimen design.

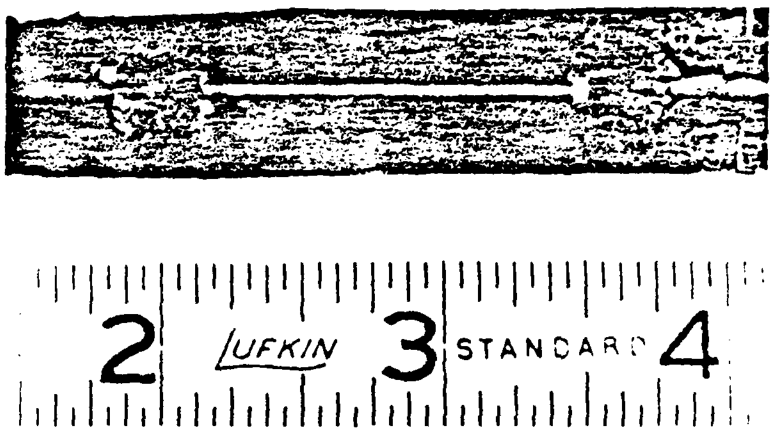

Fig. 6. Mounting of liquid-metal strain gage.

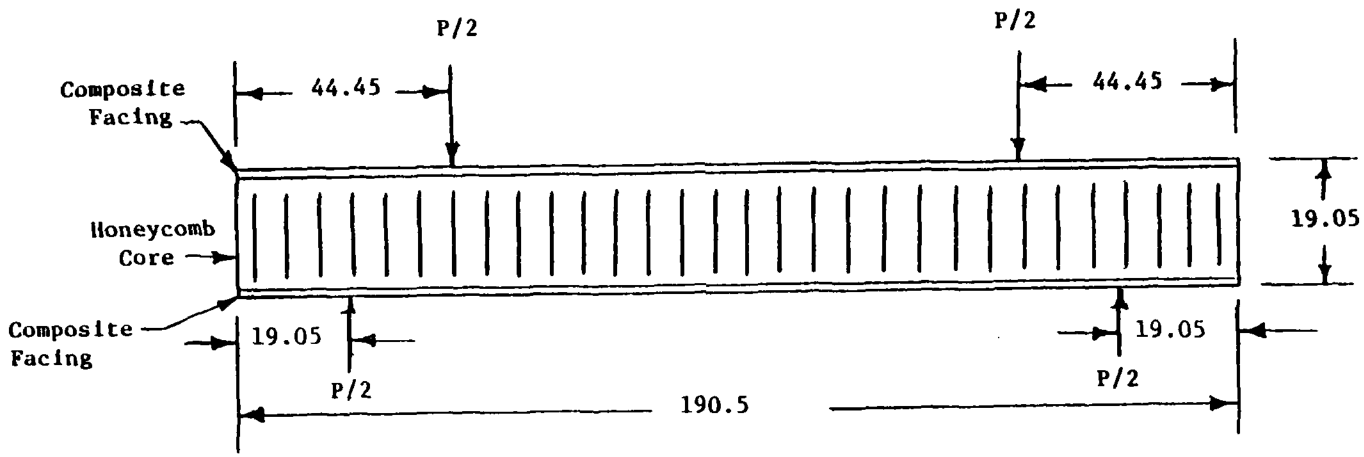

All dimensions are in mm.

Fig. 7. Dimensions of sandwich beam under four-point bending test.

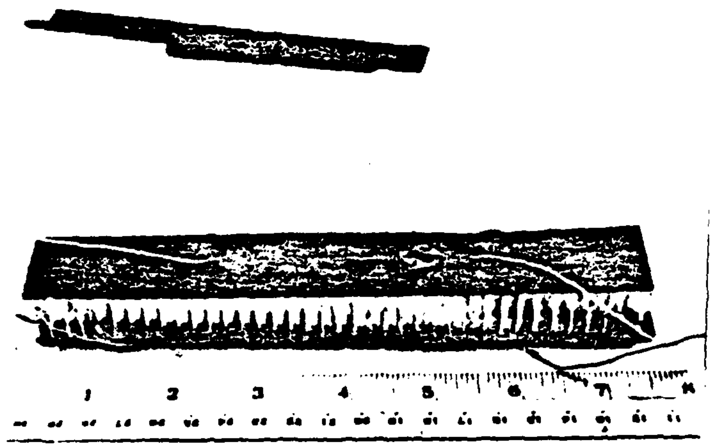

Fig. 8. Sandwich specimen.

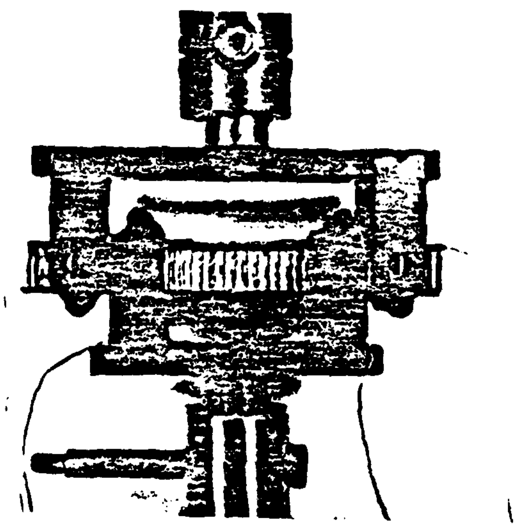

Fig. 9. Four-point bending fixture.

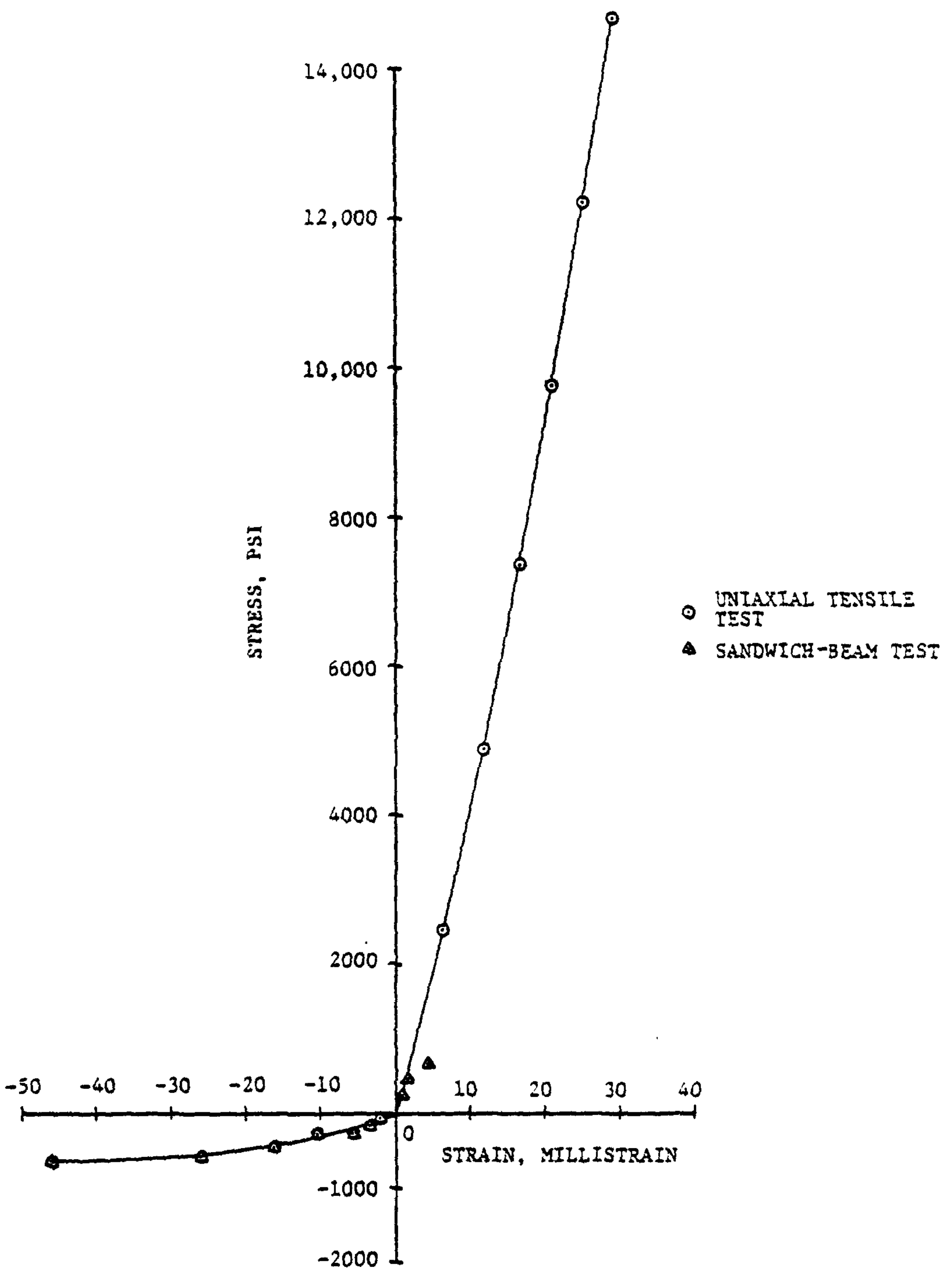

Fig. 10. Stress-strain curve for aramid-rubber in the cord direction (1 psi = 6.895×10^3 pascals).

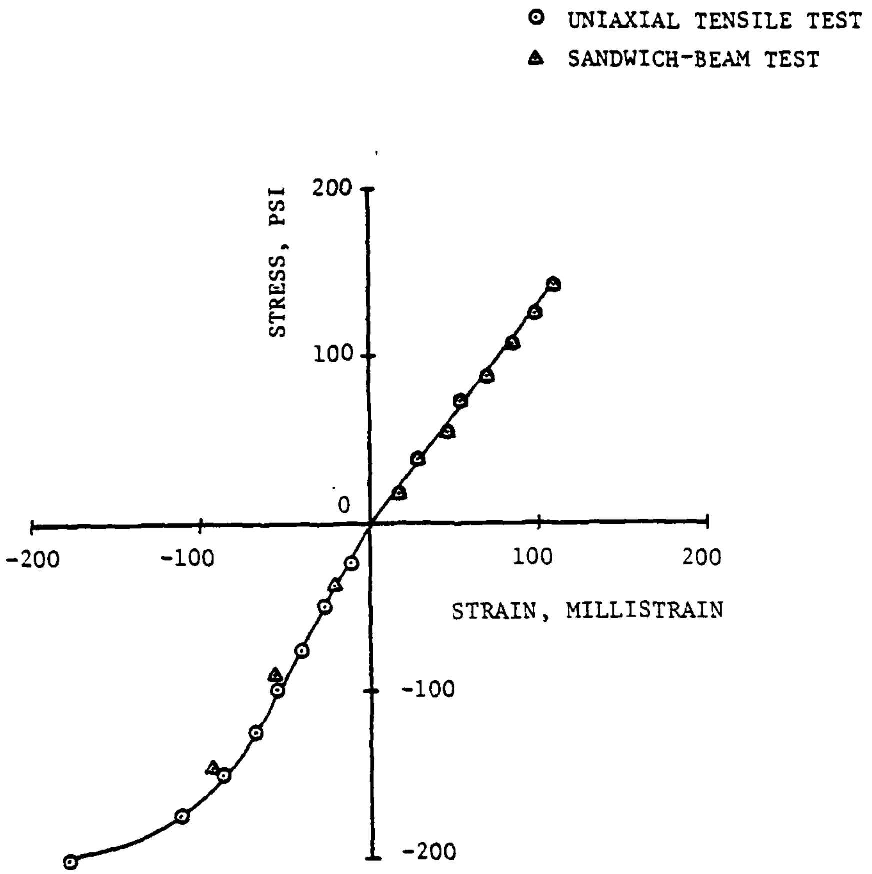

Fig. 11. Stress-strain curve for aramid-rubber in the transverse direction (1 psi = 6.895×10^3 pascals).

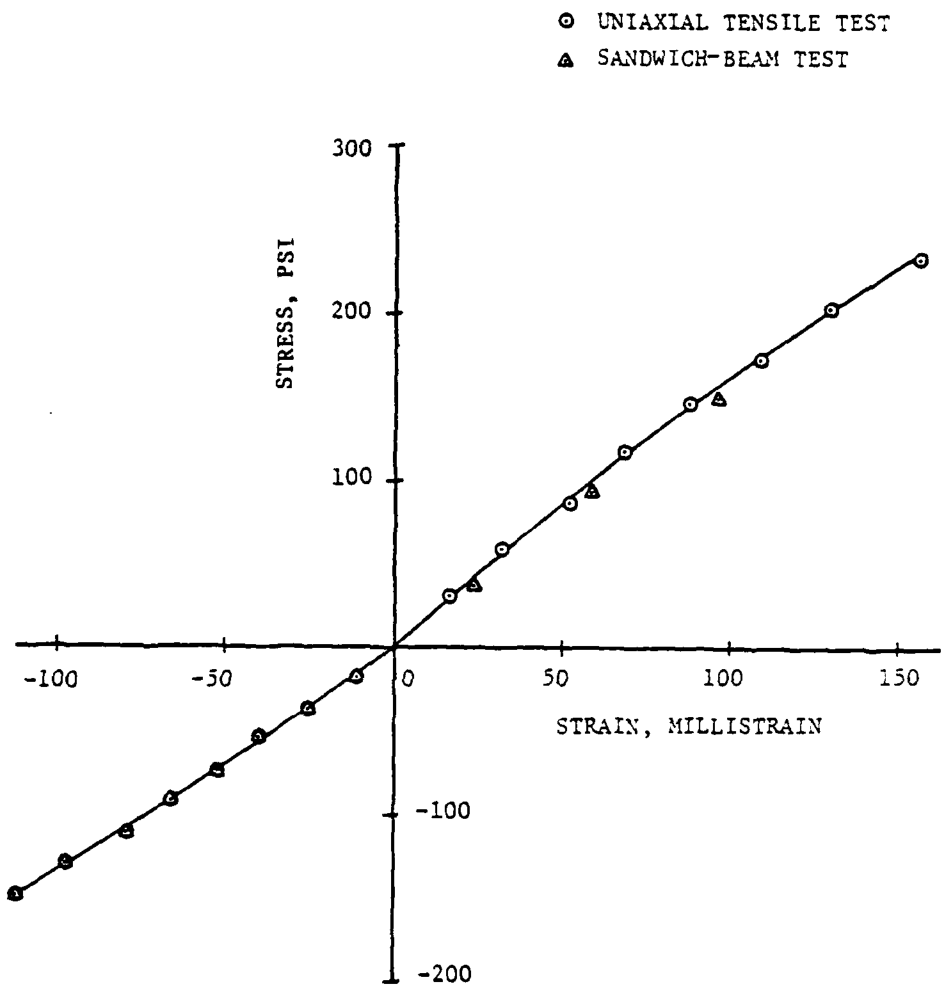

Fig. 12. Stress-strain curve for aramid-rubber at 45° to the cord direction (1 psi = 6.895 x 10^3 pascals).

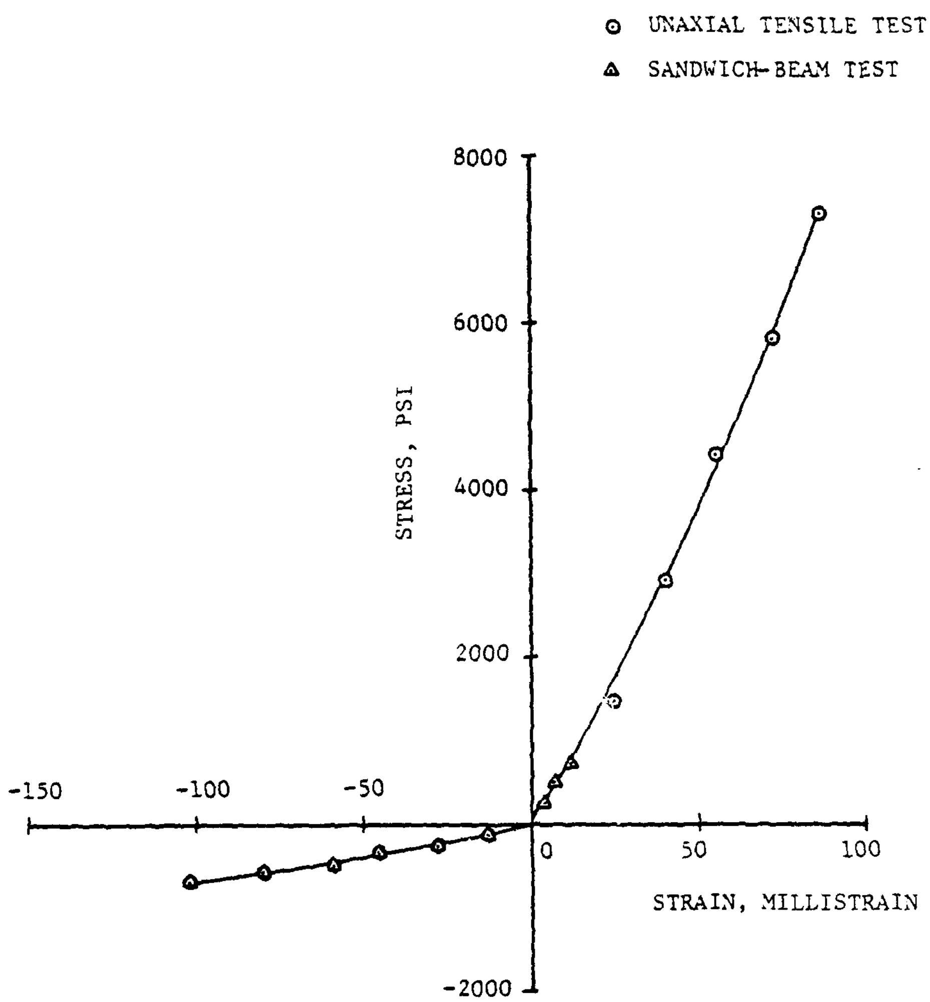

Fig. 13. Stress-strain curve for polyester-rubber in the cord direction (1 psi = 6.895 x 10^3 pascals).

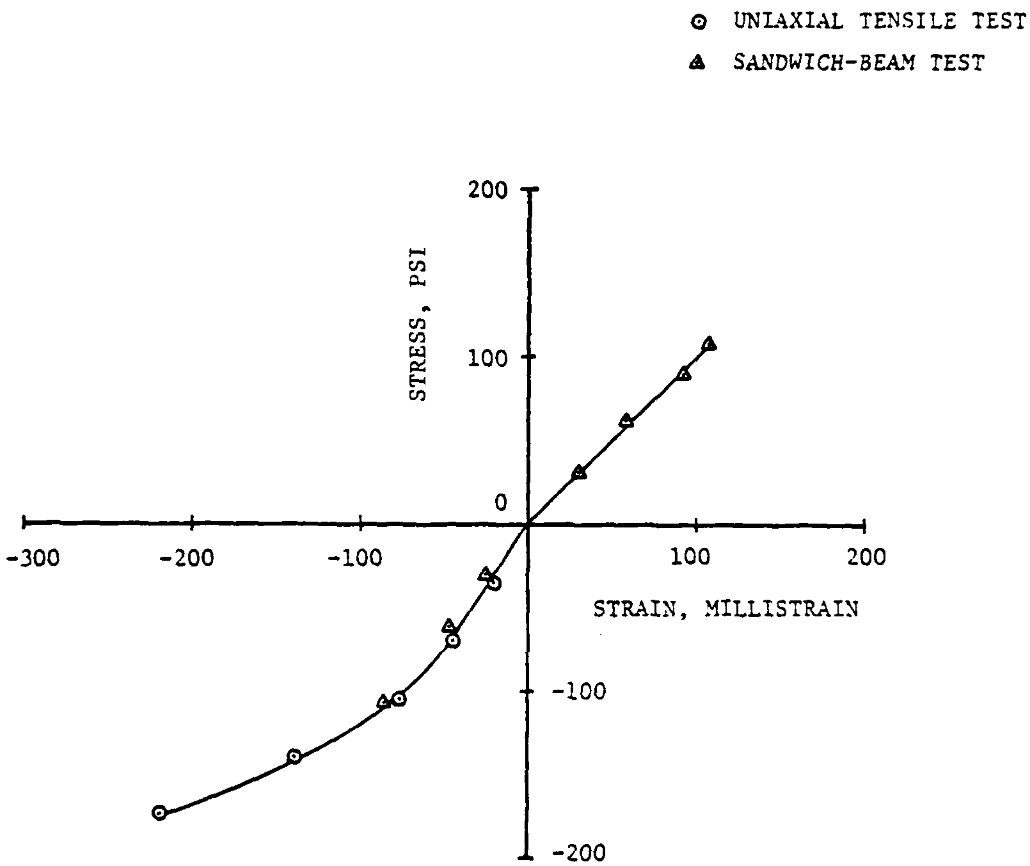

Fig. 14. Stress-strain curve for polyester-rubber in the transverse direction (1 psi = 6.895×10^3 pascals).

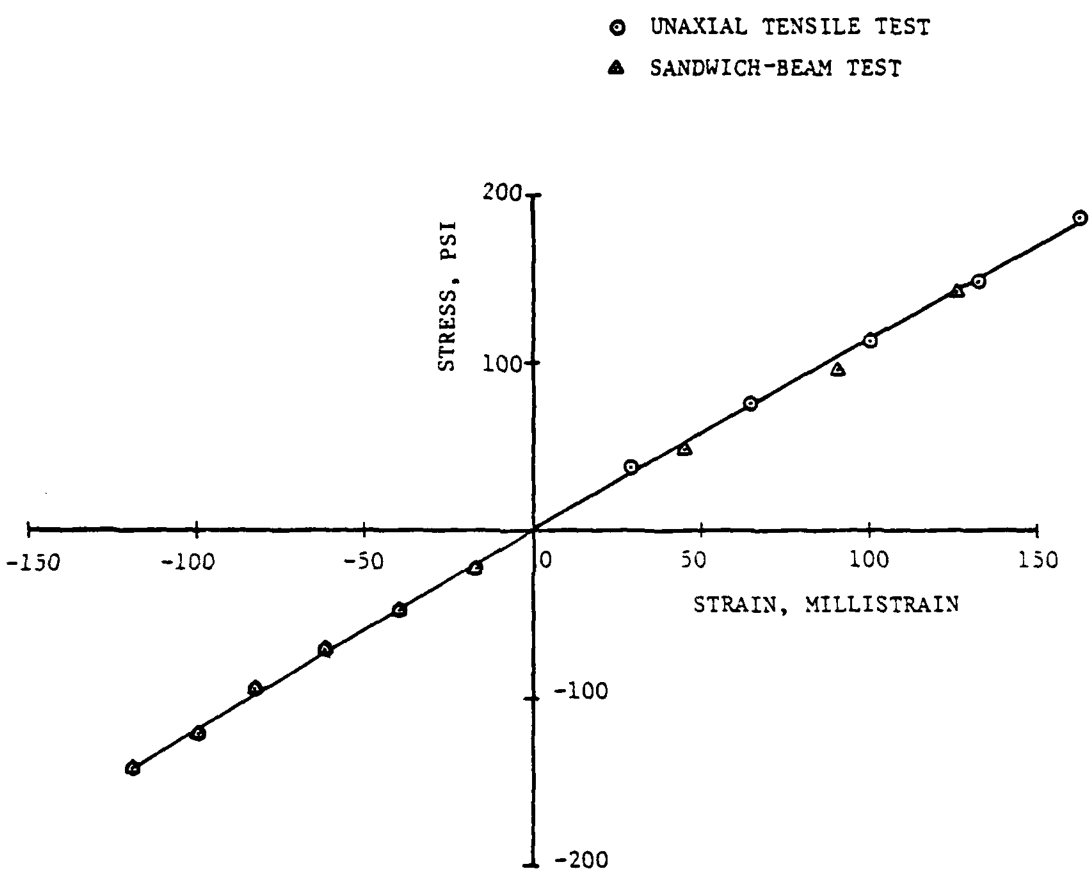

Fig. 15. Stress-strain curve for polyester-rubber at 45° to the cord direction (1 psi = 6.895 x 10^3 pascals).

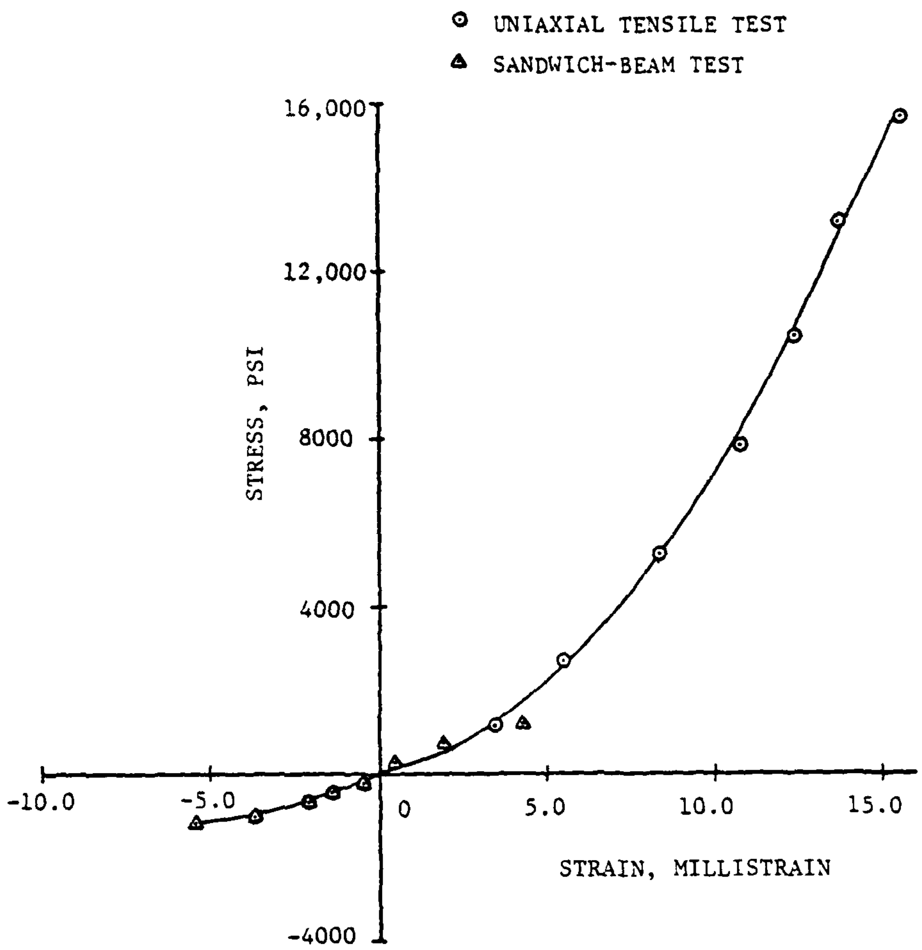

Fig. 16. Stress-strain curve for steel-rubber in the cord direction (1 psi = 6.895×10^3 pascals).

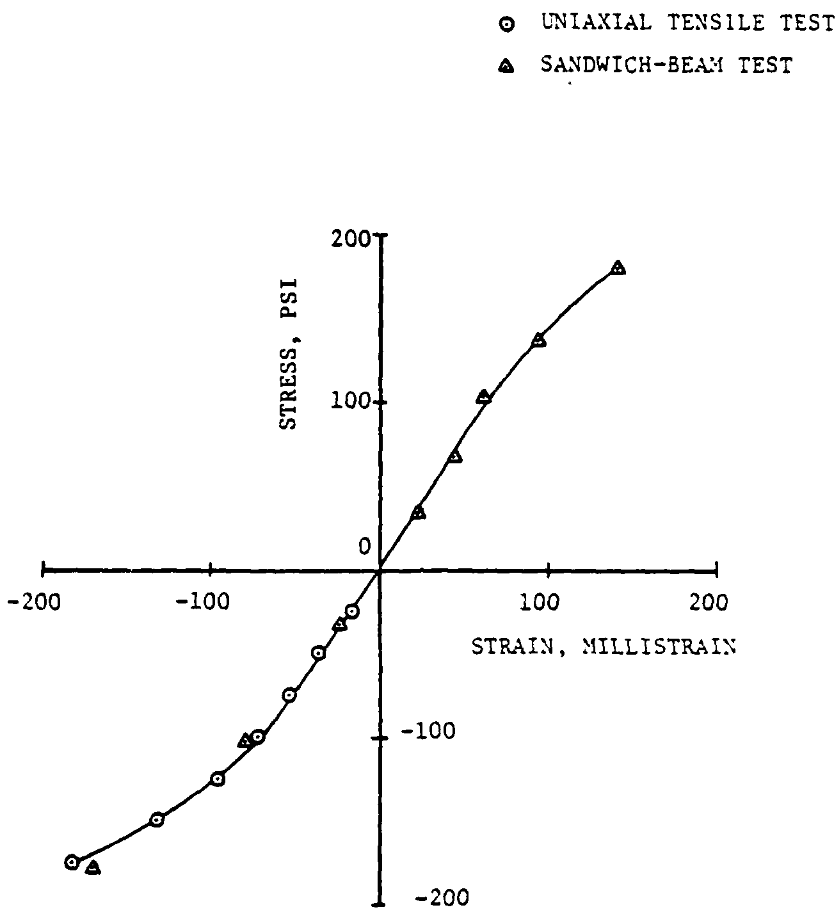

Fig. 17. Stress-strain curve for steel-rubber in the transverse direction (1 psi = 6.895×10^3 pascals).

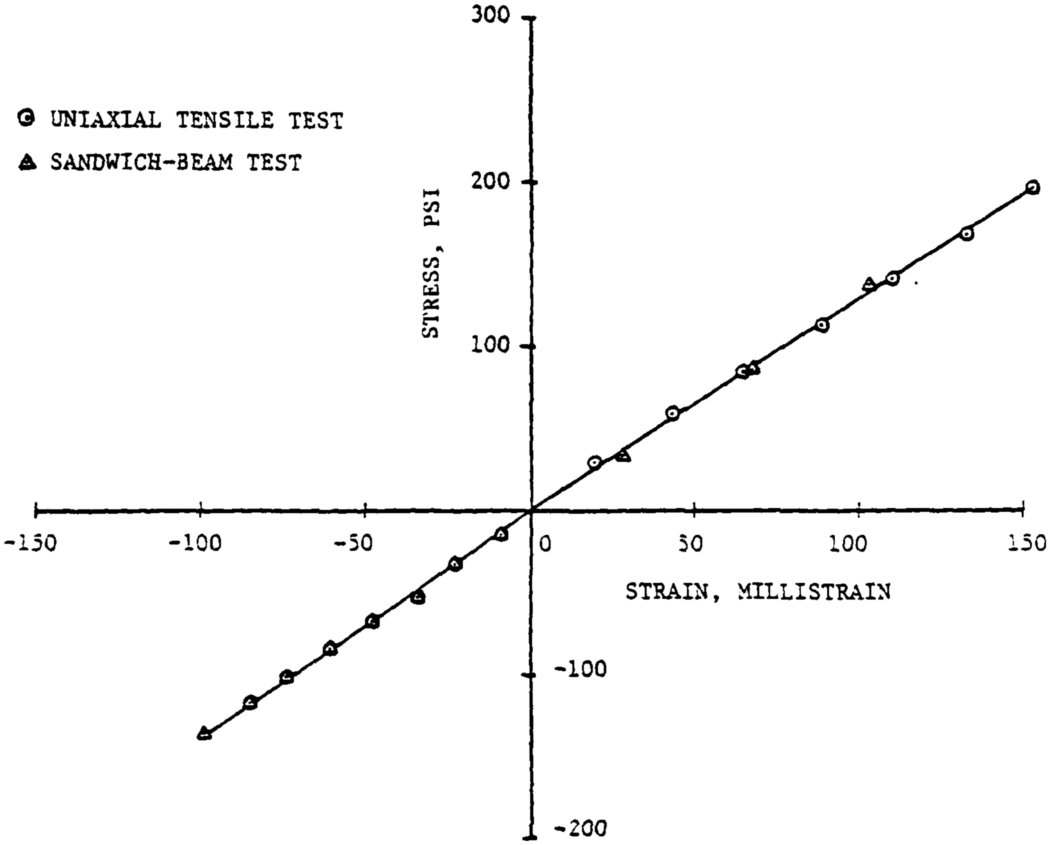

Fig. 18. Stress-strain curve for steel-rubber at 45° to the cord direction 1 psi = 6.895×10^3 pascals).

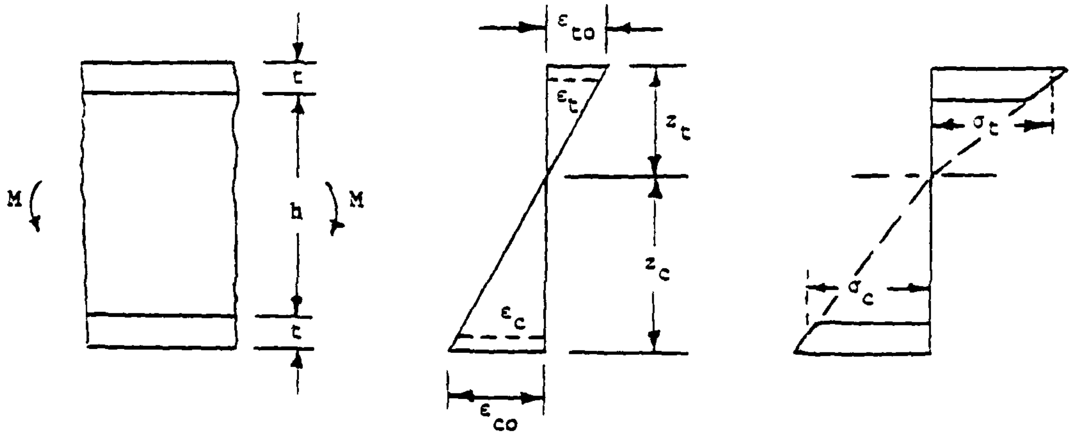

Fig. 19. Geometry, strain kinematics, and stress distribution of the sandwich-beam (ε_c, ε_{co}, z_c, and σ_c are all negative quantities).

PREVIOUS REPORTS ON THIS CONTRACT

Project Rept. No.	Issuing University Rept. No.*	Report Title	Author(s)
1	OU 79-7	Mathematical Modeling and Micromechanics of Fiber Reinforced Bimodulus Composite Material	C.W. Bert
2	OU 79-8	Analyses of Plates Constructed of Fiber-Reinforced Bimodulus Materials	J.N. Reddy and C.W. Bert
3	OU 79-9	Finite-Element Analyses of Laminated Composite-Material Plates	J.N. Reddy
4A	OU 79-10A	Analyses of Laminated Bimodulus Composite-Material Plates	C.W. Bert
5	OU 79-11	Recent Research in Composite and Sandwich Plate Dynamics	C.W. Bert
6	OU 79-14	A Penalty Plate-Bending Element for the Analysis of Laminated Anisotropic Composite Plates	J.N. Reddy
7	OU 79-18	Finite-Element Analysis of Laminated Bimodulus Composite-Material Plates	J.N. Reddy and W.C. Chao
8	OU 79-19	A Comparison of Closed-Form and Finite-Element Solutions of Thick Laminated Anisotropic Rectangular Plates (With a Study of the Effect of Reduced Integration on the Accuracy)	J.N. Reddy
9	OU 79-20	Effects of Shear Deformation and Anisotropy on the Thermal Bending of Layered Composite Plates	J.N. Reddy and Y.S. Hsu
10	OU 80-1	Analyses of Cross-Ply Rectangular Plates of Bimodulus Composite Material	V.S. Reddy and C.W. Bert
11	OU 80-2	Analysis of Thick Rectangular Plates Laminated of Bimodulus Composite Materials	C.W. Bert, J.N. Reddy, V.S. Reddy and W.C. Chao
12	OU 80-3	Cylindrical Shells of Bimodulus Composite Material	C.W. Bert and V.S. Reddy
13	OU 80-6	Vibration of Composite Structures	C.W. Bert
14	OU 80-7	Large Deflection and Large-Amplitude Free Vibrations of Laminated Composite-Material Plates	J.N. Reddy and W.C. Chao
15	OU 80-8	Vibration of Thick Rectangular Plates of Bimodulus Composite Material	C.W. Bert, J.N. Reddy, W.C. Chao, and V.S. Reddy
16	OU 80-9	Thermal Bending of Thick Rectangular Plates of Bimodulus Material	J.N. Reddy, C.W. Bert, Y.S. Hsu, and V.S. Reddy
17	OU 80-14	Thermoelasticity of Circular Cylindrical Shells Laminated of Bimodulus Composite Materials	Y.S. Hsu, J.N. Reddy, and C.W. Bert
18	OU 80-17	Composite Materials: A Survey of the Damping Capacity of Fiber-Reinforced Composites	C.W. Bert
19	OU 80-20	Vibration of Cylindrical Shells of Bimodulus Composite Materials	C.W. Bert and M. Kumar
20	VPI 81-11 & OU 81-1	On the Behavior of Plates Laminated of Bimodulus Composite Materials	J.N. Reddy and C.W. Bert
21	VPI 81-12	Analysis of Layered Composite Plates Accounting for Large Deflections and Transverse Shear Strains	J.N. Reddy
22	OU 81-7	Static and Dynamic Analyses of Thick Beams of Bimodular Materials	C.W. Bert and A.D. Tran

*OU denotes the University of Oklahoma; VPI denotes Virginia Polytechnic Institute and State University.

UNCLASSIFIED

SECURITY CLASSIFICATION OF THIS PAGE (When Data Entered)

REPORT DOCUMENTATION PAGE		READ INSTRUCTIONS BEFORE COMPLETING FORM
1. REPORT NUMBER OU-AMNE-81-8	2. GOVT ACCESSION NO. AD-A102	3. RECIPIENT'S CATALOG NUMBER 587
4. TITLE (and Subtitle) EXPERIMENTAL INVESTIGATION OF THE MECHANICAL BEHAVIOR OF CORD-RUBBER MATERIALS		5. TYPE OF REPORT & PERIOD COVERED Technical Report No. 23
		6. PERFORMING ORG. REPORT NUMBER
7. AUTHOR(s) C.W. Bert and M. Kumar		8. CONTRACT OR GRANT NUMBER(s) N00014-78-C-0647
9. PERFORMING ORGANIZATION NAME AND ADDRESS School of Aerospace, Mechanical and Nuclear Engineering University of Oklahoma, Norman, OK 73019		10. PROGRAM ELEMENT, PROJECT, TASK AREA & WORK UNIT NUMBERS NR 064-609
11. CONTROLLING OFFICE NAME AND ADDRESS Department of the Navy, Office of Naval Research Structural Mechanics Program (Code 474) Arlington, Virginia 22217		12. REPORT DATE July 1981
		13. NUMBER OF PAGES 45
14. MONITORING AGENCY NAME & ADDRESS(if different from Controlling Office)		15. SECURITY CLASS. (of this report) UNCLASSIFIED
		15a. DECLASSIFICATION/DOWNGRADING SCHEDULE

16. DISTRIBUTION STATEMENT (of this Report)

This document has been approved for public release and sale; distribution unlimited.

17. DISTRIBUTION STATEMENT (of the abstract entered in Block 20, if different from Report)

18. SUPPLEMENTARY NOTES

19. KEY WORDS (Continue on reverse side if necessary and identify by block number)

Bimodular materials, composite materials, cord-rubber composites, experimental characterization, fiber-reinforced composites, liquid-metal strain gages, mechanical behavior, nonlinear stress-strain relations, off-axis uniaxial tests, sandwich-beam tests, stress-strain behavior.

20. ABSTRACT (Continue on reverse side if necessary and identify by block number)

This report covers the experimental determination of the complete stress-strain behavior, in both fiber tension and compression, for three cord-reinforced, soft-matrix composites. These were unidirectional cord-rubber with cords of aramid, polyester, and steel. Ordinary metallic-foil strain gages could not be used because of their high stiffness relative to the matrix stiffness and because of the large strains encountered. Thus, liquid-mercury strain gages were used, and their fabrication, (over)

DD FORM 1 JAN 73 1473 EDITION OF 1 NOV 65 IS OBSOLETE

S/N 0102-014-6601

UNCLASSIFIED

SECURITY CLASSIFICATION OF THIS PAGE (When Data Entered)

20. Abstract - Cont'd

calibration, and verification are described in detail. Tests conducted included uniaxial strips for tension loading and sandwich beams for compression loading. For shear response, 45° off-axis specimens were tested. Complete discussions are presented on data-reduction procedures used, cross-checking, and comparison with data obtained by previous investigators. Simple power-law stress-strain relations are presented to depict the nonlinear stress-strain behavior, which is quite different depending upon whether the fiber strain is tensile or compressive.

DATE
FILMED

-8